ANNUAL REPORT

TO

OFFICE OF NAVAL RESEARCH

Contract USN 00024-96-I-0913

June 2000

EFFECTS OF POLLUTANTS AND MICRO-ORGANISMS ON THE ABSORPTION OF ELECTROLYTIC HYDROGEN IN IRON

H. W. Pickering

Department of Materials Science and Engineering
The Pennsylvania State University
University Park, PA 16802

PENNSTATE

1855

REPORT DOCUMENTATION PAGE

Form Approved
OMB No. 0704-0188

1. AGENCY USE ONLY (Leave blank)	2. REPORT DATE	3. REPORT TYPE AND DATES COVERED
	June 2000	Annual

4. TITLE AND SUBTITLE
Effects of Pollutants and Micro-Organisms on the Absorption of Electrolytic Hydrogen in Iron

5. FUNDING NUMBERS
USN 00014-96-I-0913

6. AUTHOR(S)
H. W. Pickering

7. PERFORMING ORGANIZATION NAME(S) AND ADDRESS(ES)
The Pennsylvania State University
Department of Materials Science and Engineering
326 Steidle Building
University Park, PA 16802

8. PERFORMING ORGANIZATION REPORT NUMBER

9. SPONSORING/MONITORING AGENCY NAME(S) AND ADDRESS(ES)
Program Officer
ATTN: A. John Sedriks, ONR 332
Office of Naval Research
Ballston Centre Tower One
800 North Quincy Street
Arlington, VA 22217-5660

10. SPONSORING/MONITORING AGENCY REPORT NUMBER

11. SUPPLEMENTARY NOTES

12a. DISTRIBUTION/AVAILABILITY STATEMENT
Approved for public release; distribution is unlimited.

12b. DISTRIBUTION CODE

13. ABSTRACT (Maximum 200 words)

The objective of this research is to define conditions under which pollutants, in particular those produced by bacteria such as sulfide end products of the SRB, affect the amount of hydrogen absorbed by iron/steel. In this current year of the project, our research focused on three related thrusts which will be reported separately below: (1) The effect of thiosulfate, which is a source of H_2S as well as other sulfur forms on hydrogen absorption into steel, (2) Modification of the IPZ analysis to include Frumkin interaction effects in order to obtain a quantitative determination of the effect of H_2S on hydrogen absorption into steels, and (3) The development and testing of an analytical procedure which requires only the readily obtainable polarization data to quantitatively characterize the HER in the same way the IPZ analysis does, but much more simply and with far less sophisticated equipment. The technique is also applicable to some other metals beside iron and steels, including nickel, stainless steel, and Cu.

14. SUBJECT TERMS			15. NUMBER OF PAGES
			16. PRICE CODE
17. SECURITY CLASSIFICATION OF REPORT	18. SECURITY CLASSIFICATION OF THIS PAGE	19. SECURITY CLASSIFICATION OF ABSTRACT	20. LIMITATION OF ABSTRACT

TABLE OF CONTENTS

Overview

The absorption of electrolytic hydrogen into the steels used in the marine industry leads to their degradation due to hydrogen embrittlement. A great deal of work has been done to investigate hydrogen embrittlement of steels. It is well accepted that once hydrogen absorption occurs that the metal or the alloy will most likely suffer from one form or another of hydrogen embrittlement. The best, well known examples are those encountered in environments where hydrogen sulfide is present such as in the presence of microorganisms, e.g., sulfate reducing bacteria (SRB) which produce hydrogen sulfide in the cycle of their metabolism.

Hydrogen absorption into metals occurs as a side reaction of the hydrogen evolution reaction (HER) on metals. This reaction occurs as a viable cathodic reaction during corrosion, cathodic protection, pickling and electroplating of metals. It is because of the multi-step nature of the HER that hydrogen absorption occurs.

In this current year of the project, our research focused on three related thrusts which will be reported separately below: (1) The effect of thiosulfate, which is a source of H_2S as well as other sulfur forms on hydrogen absorption into steel, was started last year and continued this year. (2) Modification of the Iyer-Pickering-Zamanzadeh (IPZ) analysis to include Frumkin interaction effects in order to obtain a quantitative determination of the effect of H_2S on hydrogen absorption into steels. (3) The development and testing of an analytical procedure which requires only the readily obtainable polarization data to quantitatively characterize the HER in the same way the IPZ analysis does, but much more simply and with far less sophisticated equipment. The technique is also applicable to other metals beside iron and steels, including nickel, stainless steel and Cu. In principle, the method will work on those metals and alloys for which the HER occurs by the Volmer discharge-Tafel recombination mechanism with only a few exceptions.

(1) The Relative Effects of Thiosulfate, its Decomposition Products, and its Reduction Product, H_2S on the HAR Rate in Steel

Introduction

The degrading effects of sulfur containing (thio) compounds on the integrity of metals and alloys have been well recognized (1-5). Of these compounds, the thiosulfate ion is commonly encountered in the pulp, paper, oil and gas industries and as a product of the sulfate reducing bacteria (1-3,6-11). For this reason, extensive studies have been conducted by various authors to evaluate and understand the effects of thiosulfate on the crevice corrosion (12-17), pitting corrosion (3,6,18-26), stress corrosion cracking (27-44) and anodic dissolution of metals and alloys (10,11,18-26). Furthermore, studies have focused on the electrochemistry of thiosulfate (45-51) and its adsorption behavior (27,52).

It is generally accepted that thiosulfate has a strong promoting effect on the anodic dissolution of metals (10,11,18-26). On the other hand, measurements of its effects on hydrogen absorption have been less systematic and conclusive. While some workers showed that thiosulfate solutions promote hydrogen absorption into cathodically protected steel (53), others found only a slight effect in slightly acidic solutions(27) or non detectable effect in alkaline solutions (54).

The objective of this paper is to evaluate the effects of thiosulfate ($S_2O_3^{2-}$) and sulfite (SO_3^{2-}) ions on the absorption of hydrogen into iron. Sulfites are included in this study since thiosulfate decomposes readily, in mild acidic media similar to those media encountered in pits, crevices and cracks, to give sulfite species and colloidal sulfur (see below).

Experimental

The electrochemical hydrogen permeation technique, similar to that used by Frumkin (55) and by Devanathan and Stachurski (56), was used in this study to collect data on both the HER and HAR on iron (steel) membranes in sulfate solutions containing

different thiosulfate or sulfite ion concentrations. The steel membranes of 0.25 mm thickness were obtained from Goodfellow with the following composition: Mn, 0.3%; Si, 0.1%; C, <0.08%; S, < 0.05% and the balance, Fe. They were polished to 0.5 μm alumina, degreased in acetone, washed with double distilled water, and subsequently annealed in pure hydrogen at 900°C for 2hrs in a tube furnace, followed by a furnace cool in the same atmosphere. Solutions of 0.1N H_2SO_4 + 0.9N Na_2SO_4 (pH 1.8) and 1N Na_2SO_4 (pH 7) were used throughout this study. All solutions were prepared from analytical grade chemicals and double distilled water. Before admitting the solutions to the cell, they were pre-electrolyzed (Pt electrodes) at 3 mA for 2 hours under deaeration using hydrogen to remove impurities that could otherwise affect the quality of the data. These solutions were then used as blank solutions to which the different concentrations of thiosulfate or sulfite ions were added. The solutions were subsequently deaerated with hydrogen. One surface of the membrane was coated with electroless palladium using Pallamerse solution before the membrane was mounted in the cell. The areas of the input and exit surfaces were 0.8 cm^2. The exit cell contained 0.1N NaOH and the Pd coated side of the membrane. The latter was potentiostated at 0.150 mV (Hg/HgO) to ensure complete oxidation of the dissolved hydrogen diffusing through the membrane. Further details about the experimental setup are reported elsewhere (57).

Results and Discussions

Fig. 1 shows the effect of thiosulfate concentration on the hydrogen permeation transients through the steel membranes. Note the profound effect of the concentration of thiosulfate in the 0.1N H_2SO_4 + 0.9N Na_2SO_4 (blank) solution on the permeation current, i_p. A 0.1 mM thiosulfate addition to the blank solution increases the steady permeation current obtained after the short transient period, i_∞, by about 2 fold, while the solution which is 10 mM in thiosulfate increases i_∞ by about 6 fold over the blank solution. This demonstrates that thiosulfate ion enhances hydrogen absorption into steel in acidic (pH 1.8) thiosulfate containing solution.

In addition to enhancing hydrogen absorption into steel, thiosulfate enhances the HER in the pH 1.8 solution. Fig. 2 shows the Tafel plots of the HER obtained on the steel

at different thiosulfate ion concentrations ($\eta = E - E^{eq}$, $E^{eq} = -0.349$ V (SCE)). This figure shows that an increasing thiosulfate ion concentration enhances the HER, i.e., the hydrogen overpotential decreases, at the same value of the applied cathodic charging current, for increasing thiosulfate concentrations.

In acidic media, thiosulfate readily decomposes to give colloidal sulfur and sulfurous acid (3 ,12,13),

$$S_2O_3^{2-} + 2H^+ \rightarrow S + H_2SO_3 \qquad (1)$$

Consequently, the increase in i_∞ may be attributed to one or more of the following: any remaining thiosulfate ions, the colloidal sulfur and/or the sulfurous acid. As a start to sorting out these different possibilities, some experiments were carried out on thiosulfate in a neutral medium, where reaction 1 is not likely to occur and the only one of these species in solution is the thiosulfate ion (13,58,59). The hydrogen permeation transients in the neutral medium are shown in Fig. 3. This figure shows that thiosulfate in the neutral medium increases the rate of hydrogen absorption within iron. A concentration of 0.1 mM of thiosulfate ion increases i_∞ by about 2 fold while the 10 mM concentration increases i_∞ by about 3 fold. This increase in the hydrogen absorption reaction in the neutral solution was accompanied by an increase in the hydrogen evolution reaction kinetics. Fig. 4 shows the polarization plots obtained on iron in 1N Na_2SO_4 solution at different thiosulfate ion concentrations ($\eta = E - E^{eq}$, $E^{eq} = -0.661$ V (SCE)). This figure reveals that thiosulfate enhances the HER, i.e., the hydrogen overpotential at the same value of the applied cathodic charging current decreases with increasing concentration of thiosulfate. The value of current (i_c and i_∞) obtained for the blank solution (Figures 2 and 4, respectively) agree well with those in the literature at the same pH (57).

Comparison of Figs. 1 and 3 reveals that the rate of hydrogen permeation within iron is greater in an acidic than in a neutral medium, for both the blank solution and the blank solution plus a given amount of thiosulfate (or its decomposition products). The increase in i_∞ produced by the thiosulfate is also greater in the acid solution. This points to a possible enhancing effect also by the decomposition products of thiosulfate on hydrogen permeation. To test this hypothesis, experiments were run in the presence of

solely SO_3^{2-} in the acidic medium (pH 1.8) at the same concentrations as in the thiosulfate experiments. Fig. 5 shows the effect of the concentration of the sulfite ions on the hydrogen permeation transient. The figure shows that the SO_3^{2-} ions cause an increase in the steady state hydrogen permeation current density. This increase in the hydrogen absorption rate in the presence of sulfite ions is also coupled with an increase in the HER kinetics, see Fig. 6.

The extent of the enhancement in the hydrogen permeation rate at different thiosulfate or sulfite concentrations may be expressed quantitatively by an enhancement factor, ε

$$\varepsilon = \frac{i_\infty(additive)}{i_\infty(blank)} \tag{2}$$

where i_∞(additive) and i_∞(blank) are the steady state hydrogen permeation current densities for the solution with the additive and the blank solution, respectively. Table 1 lists the values of the steady state hydrogen permeation current, i_∞, and the enhancement factor, ε, for different concentrations of thiosulfate and sulfite ions in acidic and neutral solutions. It reveals that the thiosulfate (and/or its decomposition products) in acid medium show a high promoting effect (larger ε) than sulfite ions at the same concentration. If one assumes that 1 mole of sulfite results from the decomposition of one mole of thiosulfate, one concludes that the resulting colloidal sulfur also causes a small enhancement of the hydrogen absorption, although another possibility exists and is discussed below. In addition, the thiosulfate was found to promote hydrogen absorption into iron in a neutral medium but to a lesser extent than its reaction products in acidic solutions.

In addition to their catalytic effect in enhancing the hydrogen evolution and absorption reactions on iron, $S_2O_3^{2-}$, SO_3^{2-} and S are thermodynamically unstable and, therefore, tend to be reduced on the metal surface to H_2S. Hydrogen sulfide is well known to enhance hydrogen absorption into metals (1, 61-70) and also to enhance the HER (71-73). However, the reduction of these sulfide species involves multi-step reactions which makes them kinetically unfavorable. Thus, only trace amounts of H_2S can be expected to

be present in the solution, i.e., the contribution of electrochemical reduction of thiosulfate and/or its decomposition products to the measured cathodic currents in the polarization curves (Figs. 2, 4, and 6) is insignificant as has been shown in the literature (13). Even very small amount of H_2S, however, could contribute to the observed enhanced hydrogen absorption (74).

Conclusions

Thiosulfate causes an enhancement of the hydrogen absorption and evolution reactions in acidic solutions. The enhancement of the HAR was attributed mainly to one of its decomposition products (sulfurous acid), since thiosulfate is readily decomposed in acidic media to sulfite ions and sulfur, and since results with solely sulfite ions in the same acidic (blank) solution show only somewhat less enhancement of the HAR. Thiosulfate in neutral solution, where it remains mainly as undecomposed thiosulfate, also causes enhancement of the hydrogen absorption reaction but to a much lesser extent. Thus, it is concluded that the major effect of thiosulfate on the HAR is due to its decomposition product, SO_3^{2-} in acidic media and to thiosulfate, itself, in neutral media. The mechanism of the enhancement is not known and could alternatively involve the reduction product of thiosulfate and its decomposition products, H_2S.

References

1. P. R. Rhodes, in H_2S Corrosion in Oil and Gas Production, R. N. Tuttle and R. D. Kane, editors, NACE, TX (1991).

2. J. S. Smith and J. D. A Miller, Br. Corros. J., **136**, 10 (1975)

3. G. Cargnolino and O. H. Tuovinen, Intern. Biodetrior. J., **20**, 9 (1984).

4. P. Sury, Corros. Sci., **16**, 879 (1979).

5. G. Schmitt, Corrosion, **47**, 285 (1991).

6. R. C. Newman, Corrosion, **41**, 450 (1985).

7. R. C. Newman and K. Sieradzki, Corros. Sci, **23**, 363 (1983).

8. A. Garner, Pulp and Paper Canada, **83**, 20 (1982).

9. H. H. Horowitz, Corros. Sci., **23**, 353 (1983).

10. T-L. Yau, Mater. Perform., **32**, 65 (1993).

11. C. E. Jaske and A. P. Castillo, Mater. Perform, **26**, 37 (1987).

12. S. J. Mulford and D. Tromans, Corrosion, **44**, 891 (1988).

13. D. Tromans and L. Frederick, Corrosion, **40**, 633 (1984).

14. S. E. Lott and R. C. Alkire, J.Electrochem.Soc., **136**, 973 (1989).

15. R. C. Alkire and S. E. Lott, J.Electrochem. Soc., **136**, 3256 (1989).

16. H. S. Isaacs, B. Vyas, and M. W. Kendig, Corrosion, **38**, 130 (1982).

17. C. S. Brossia and R. G. Kelly, Corrosion, **54**, 145 (1998).

18. R. C. Newman, H. S. Isaacs, and B. Alman, Corrosion, **38**, 261 (1982).

19. R. C. Newman, W. P. Wong, H. Ezuber, and Garner, Corrosion, **45**, 282 (1989)

20. A. Garner, Corrosion, **41**, 587 (1985).

21. C. Duret-Thual, D. Costa, W. P. Yang and P. Marcus, Corros. Sci., **39**, 913 (1997).

22. R. Roberge, Corrosion, **44**, 274 (1988).

23. R. C. Newman, W. P. Wong, and A. Garner, Corrosion, 42, 489 (1986).

24. J. T. Ho, G. P. Yu, Corrosion, **48**, 147 (1992).

25. P. R. Roberge, S. Wang, and R. Roberge, Corrosion, **52**, 733 (1996).

26. A. R. J. Kucernak, R. Peat, and D. E. Williams, J.Electrochem.Soc., **139**, 2337 (1992).

27. H. H. Horowitz, J. Electrochem. Soc., **132**, 2064 (1985).

28. R. C. Newman and K. Sieradzki, Corros.Sci., **23**, 363 (1983).

29. G. Cragnolino, D. D. Macdonald, Corrosion, **38**, 406 (1982).

30. H. S. Issacs, B. Vyas, and M. W. Kendig, Corrosion, **38**, 130 (1980).

31. E. A. Ashour, E. A. Abd El Meguid, and B. G. Ateya, Corrosion, **53**, 612 (1997).

32. D. B. Wells, J. Stewart, R. Davidson, P. M. Scott, and D. Williams, Corros.Sci., **33**, 39 (1992).

33. H. S. Isaacs, J. Electrochem.Soc., **135**, 2180 (1988)

34. W-T. Tsai, C-S. Chang, and J-T. Lee, Corrosion, **50**, 98 (1994).

35. I. Y. Yang, Corrosion, **49**, 576 (1993).

36. T. Shibata and Huruna, J. Iron and Steel Inst. of Japan, **78**, 312 (1992).

37. W-T. Tsai, M-J. Sheu, and J-T. Lee, Corros. Sci., **38**, 33 (1996).

38. P. M. Perillo and G. S. Duffo, Corrosion, **46**, 545 (1990).

39. T. Shibata and Huruna, Corros. Eng. Japan, **41**, 217 (1992).

40. J. K. Lee and Z. Smialowska-Szklarska, Corrosion, **44**, 560 (1988).

41. L. G. Ljungberg, D. Cubicciotti, and M. Trolle, Corrosion, **45**, 215 (1989).

42. R. Bandy and R. L. Sabatini, Corrosion, **41**, 242 (1985).

43. S. S. Hsu, S. C. Tsai, J. J. Kai, and C. H. Tsai, J. Nuc. Mater. (The Netherlands), **184**, 97 (1991).

44. J.J. Kai, C. H. Tsai, T. A. Huang, and M. N. Liu, Metall. Trans. A, **20**, 1077 (1989).

45. P. Marcus and E. Protopopoff, Corros. Sci., **39**, 1741 (1997).

46. P. Marcus and E. Protopopoff, J. Electrochem. Soc., **137**, 2709 (1990).

47. P. Marcus and E. Protopopoff, J. Electrochem. Soc., **140**, 1571 (1993).

48. P. Marcus and E. Protopopoff, J. Electrochem. Soc., **140**, 15861 (1997).

49. R. J. Biernat and R. G.Robins, Electrochimica Acta, **14**, 809 (1969).

50. R. C. Murray, J. Electrochem. Soc., **130**, 866 (1983).

51. T. Hemmingsen, Electrochim. Acta, **37**, 2775 (1992), **37**, 2785 (1992).

52. A. E. Thomas, Y-E. Sung, M. A. Gamboa, K. Franaszczuk and A. Wieckowski, J. Electrochem. Soc., **142**, 476 (1995), **144**, 582 (1997).

53. R. P. Hu, P. Manolatos, M. Jerome, M. Meyer, and J. Galland, Corros. Sci., **40**, 619 (1998).

54. C. C. Juang and J. K. Wu, Corros.Sci., **36**, 1727 (1994).

55. A. N. Frumkin and N. Aladyalova, Acta Physicochim (USSR), **19**, 1 (1944).

56. M. A.Devanathan and Z. Stachurski, Proc. Roy. Soc. Chem., **A270**, 90 (1962).

57. M. H. Abd Elhamid, B. G. Ateya and H. W. Pickering, J. Electrochem. Soc., **144**, L58 (1997).

58. N. V. Sidgwick in The Chemical Elements and Their Compounds, V.2, p.917, Oxford University Press, London (1950).

59. T. Moeller, in Inorganic Chemistry, p.542, John Wiley and Sons, New York, (1952).

60. M. Pourbaix, in Atlas of Electrochemical Equilibria in Aqueous Solutions, p.545, Pergamon Press (1966).

61. S. Y. Tsai and H. C. Shih, J. Electrochem. Soc., **145**, 1968 (1998).

62. M. S. Cayard and R. D. Kane, Corrosion, **53**, 237 (1997).

63. H. Asahi, M. Ueno, and T. Yonezama, Corrosion, **50**, 537 (1994).

64. F. Elshawesh and J. C. Scully, Brit. Corros., **33**, 49 (1998).

65. B. J. Berkowitz and H. H. Horowitz, J. Electrochem. Soc., **129**, 468 (1982).

66. M. D. Tumulura, Mater. Perform., **24**, 38 (1985).

67. T. V. Venkatasubramanian and T. J. Baker, Met. Sci., **18**, 241 (1981).

68. R. G. J. Edyvean, Intern. Biodeterior. J., **27**, 109 (1991).

69. L. W. Tsay, W. L. Lin, S. W. Cheng, and G. S. Leu, Corros. Sci., **39**, 1165 (1997).

70. H. S. Cambell and R. Francis, Brit. Corros., **30**, 154 (1995).

71. A. Kawashima, K. Hashimoto, and S. Shimodaira, Corrosion, **32**, 321 (1976).

72. Z. A. Iofa and F. L. Kam, Protection of Metals, **10**, 12 (1974).

73. R. N .Iyer, I. Takauchi, M.Zamanzadeh and H. W. Pickering, Corrosion, **46**, 360 (1990).

74. Y. Saio and K. Nobe, Brit. Corros., **30**, 119 (1995)

List of Figures

Table 1: Effects of the concentrations of thiosulfate (TS) and sulfite ions on the hydrogen permeation rate within iron and the enhancement factor, ε, in acidic (pH 1.8) and neutral (pH 7) solutions at a charging current of 1.25 mA cm^{-2}.

C,mM TS	$S_2O_3^{2-}$ pH=1.8		SO_3^{2-} pH=1.8		$S_2O_3^{2-}$ pH=7	
	i_∞ μA cm^{-2}	ε	i_∞ μA cm^{-2}	ε	i_∞ μA cm^{-2}	ε
0	3.2	1	3.2	1	0.8	1
0.1	6.6	2.0	5.9	1.8	1.3	1.6
1	14.0	4.3	12.4	3.8	1.7	2.1
10	20.4	6.3	16.8	5.2	2.2	2.8

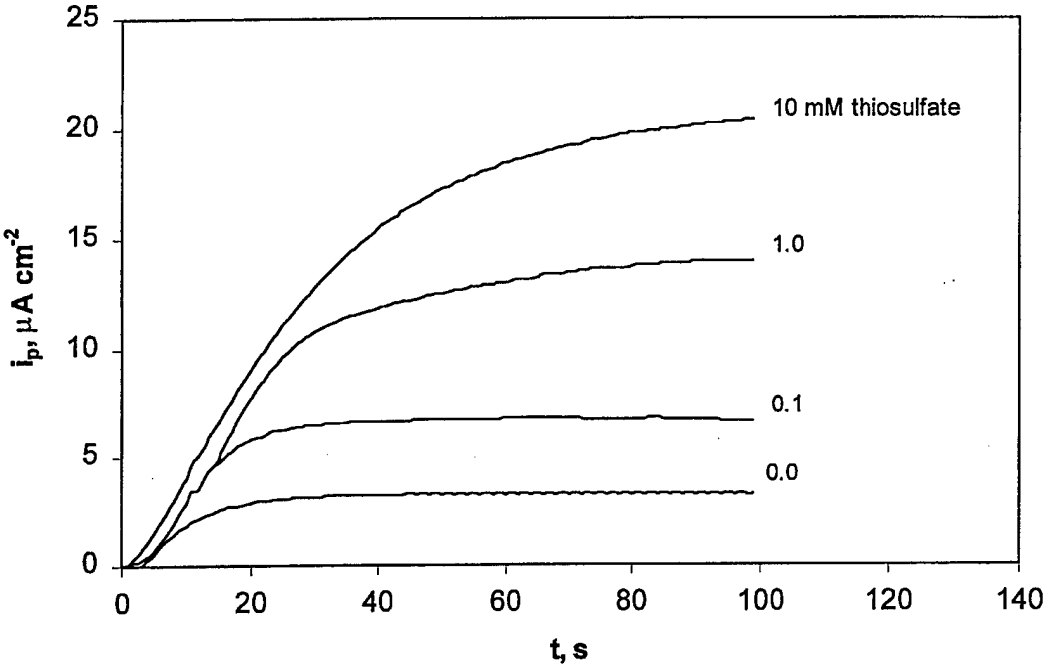

Fig. 1: Effect of thiosulfate ion concentration on the hydrogen permeation transients obtained on a steel membrane of thickness 0.25 mm in 0.1N H_2SO_4 + 0.9N Na_2SO_4 (pH 1.8) at a charging current density of 1.25 mA cm^{-2}.

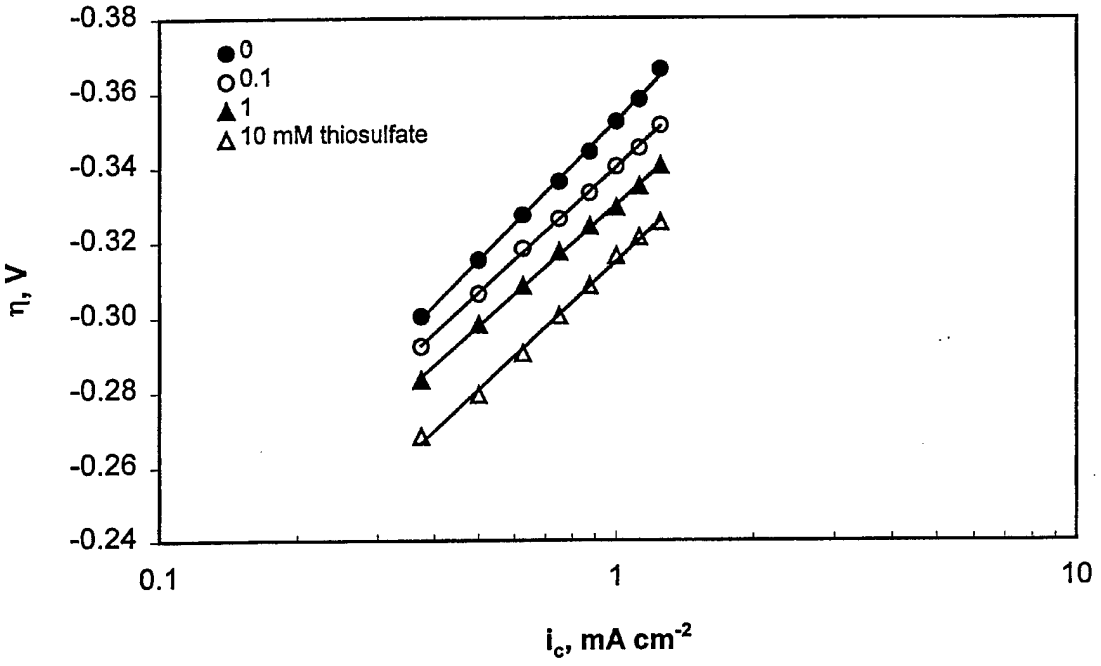

Fig. 2: Effect of thiosulfate ion concentration on the Tafel plots of the HER obtained on a steel membrane of thickness 0.25 mm in 0.1N H_2SO_4 + 0.9N Na_2SO_4.

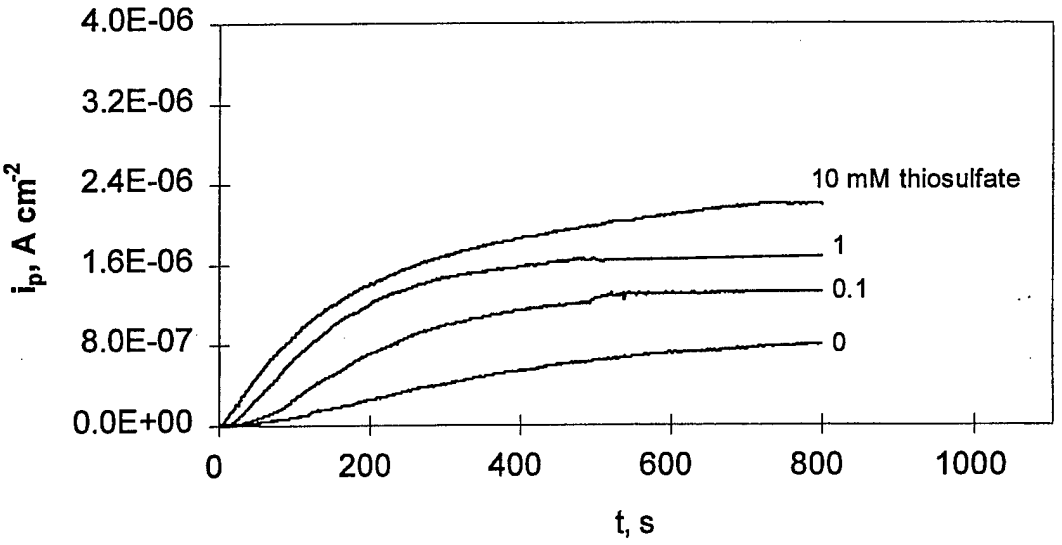

Fig. 3: Effect of thiosulfate ion concentration on the hydrogen permeation transients obtained on a steel membrane of thickness 0.25 mm in 1N Na_2SO_4 (pH 7) at a charging current density of 1.25 mA cm^{-2}.

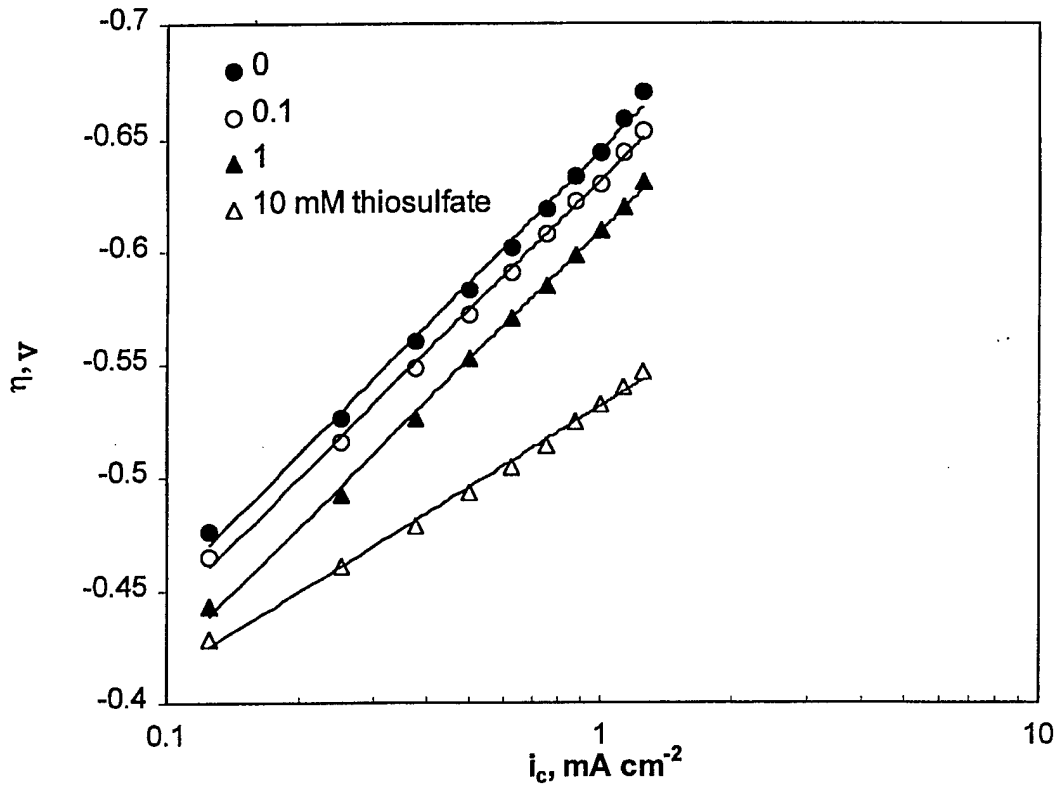

Fig. 4: Effect of thiosulfate ion concentration on the Tafel plots of the HER obtained on a steel membrane of thickness 0.25 mm in 1N Na_2SO_4.

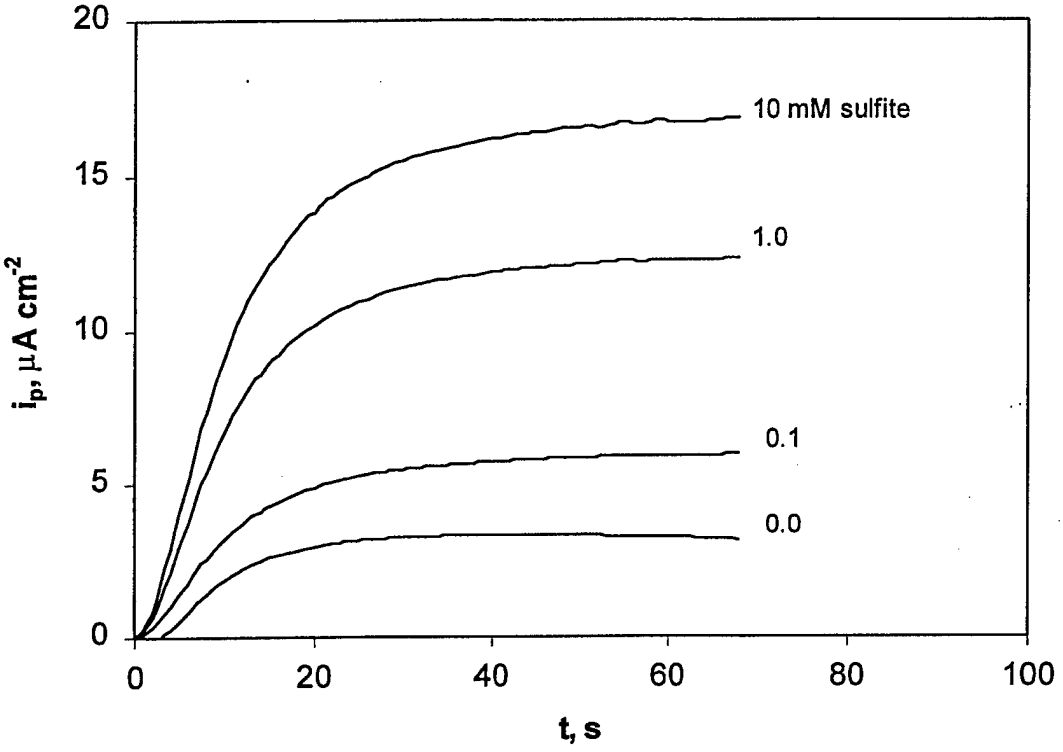

Fig. 5: Effect of sulfite ion concentration on the hydrogen permeation transients obtained on a steel membrane of thickness 0.25 mm in 0.1N H_2SO_4 + 0.9N Na_2SO_4 (pH 1.8) at a charging current density of 1.25 mA cm^{-2}.

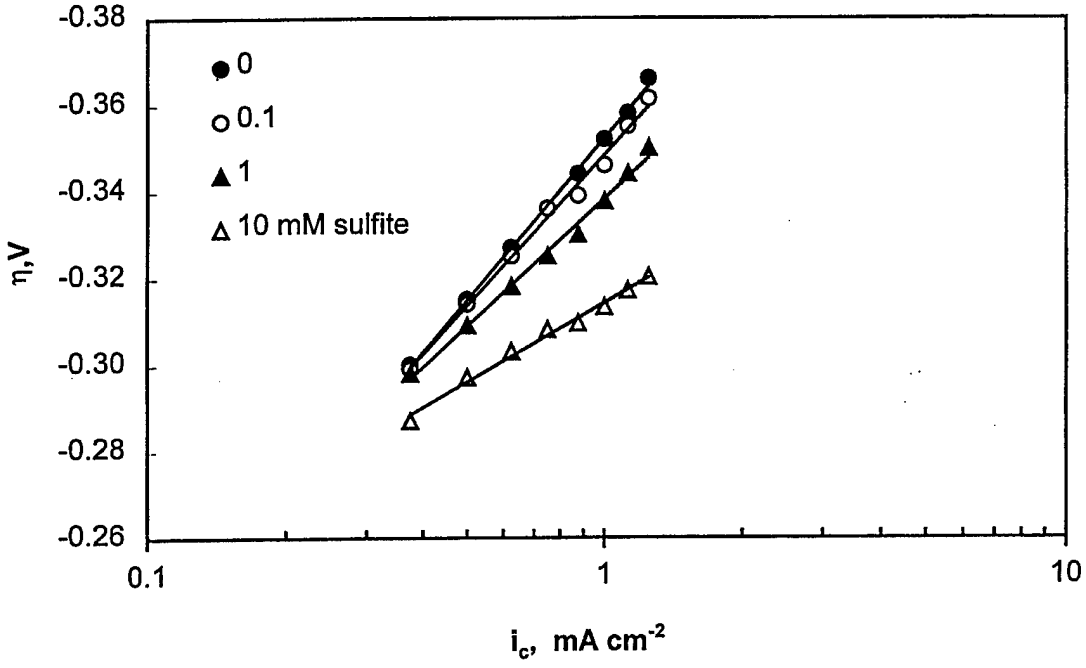

Fig. 6: Effect of sulfite ion concentration on the Tafel plots of the HER obtained on a steel membrane of thickness 0.25 mm in 0.1N H_2SO_4 + 0.9N Na_2SO_4 at a charging current density of 1.25 mA cm^{-2}.

(2) A Modified IPZ Analysis for Quantitative Determination of the Effect of H_2S on the Rate Constant of the HAR and HER for Steel

Model Highlights

It was found during analysis of the experimental data that the data collected in the presence of the sulfur containing compounds such as thiosulfate and hydrogen sulfide did not fit the requirements of the original Iyer-Pickering-Zamanzadeh (IPZ) analysis, confirming this finding for H_2S in a prior study (1). To overcome this difficulty, additional modeling analysis was performed in the past quarter in order to expand the applicability of the IPZ analysis. This effort was successful and resulted in a generalized IPZ analysis that could be applied to the data reported below. The model development follows.

Assuming a couple discharge-recombination mechanism for the HER, the following reactions take place in the charging compartment of the permeation cell, i.e.,

$$H^+ + e^- \xrightarrow{k_1} M - H_{ads} \tag{1}$$

$$M - H_{ads} + M - H_{ads} \xrightarrow{k_2} H_2 \tag{2}$$

where $M - H_{ads}$ is an adsorbed hydrogen atom on the membrane surface. Some of the adsorbed hydrogen atoms will absorb (H_{abs}) into the iron and quickly establish the back equilibria.

$$M - H_{ads} \underset{k_{des}}{\overset{k_{abs}}{\longleftrightarrow}} H_{abs} + M \tag{3}$$

The absorbed hydrogen will diffuse through the iron membrane at a steady rate given by (1-7)

$$i_\infty = Fk_{abs}\theta_H - Fk_{des}C_H^\circ \tag{4}$$

The original IPZ analysis (7) developed three major relationships between the hydrogen evolution reaction (HER) and the hydrogen adsorption reaction (HAR). The first one is between the steady state hydrogen permeation current density, i_∞, and the hydrogen recombination current density, i_r. This relation is shown in Equation 5. Earlier, others (8) had predicted this proportionality and found it to hold in different solutions. Another relationship is between the charging function, $i_c\exp(a\alpha\eta)$, and i_∞ which is shown in Equation 6. The last one is between i_∞ and the hydrogen surface coverage , θ_H, shown in Equation 7.

$$i_\infty = k\sqrt{\frac{F}{k_2}} * \sqrt{i_r} \tag{5}$$

$$i_c\exp(a\alpha\eta) = i_o' - \frac{i_o'}{Fk} i_\infty \tag{6}$$

$$i_\infty = Fk\theta_H \tag{7}$$

where i_c is the charging current density, $i_o' = Fk_1C_{H+} = i_o/(1-\theta_H^e)$, i_o is the exchange current density of the HER and θ_H^e is the hydrogen surface coverage at equilibrium, C_{H^+} is the hydrogen ion concentration in the electrolyte, a = F/RT where F, R and T have their usual meanings, α is the transfer coefficient, η is the overpotential of the HER, and k is the kinetic-diffusion constant and is defined as

$$k = \frac{k_{abs}}{1 + k_{des}\frac{L}{D}} \tag{8}$$

where D is the hydrogen diffusion coefficient within the metal and L is the membrane thickness. All three of these relationships have been found to hold in some experimental systems (7-9) Equation 7 is a modified version of Equation 4a in the original IPZ analysis and was recently derived by Ramasubramanian, et al. (9). More details about the IPZ analysis can be found elsewhere (7, 10). For the local equilibrium of the intermediate

absorption-desorption reaction, the concentration of hydrogen inside the metal is obtained as (4).

$$C^{o} = k\,\theta_H\,L/D \tag{9}$$

The original IPZ analysis (7) assumes the Langmuir adsorption isotherm. However, data collected using the hydrogen permeation technique for the iron/H_2S-acid system in the present work did not satisfy the requirement of Equation 5 in the original IPZ analysis (7), as found previously by Iyer, et. al. (1). The Frumkin adsorption isotherm then was used to develop a generalized IPZ analysis, following on the initial progress in this direction by Iyer, et. al. (1, 10). According to Reactions 1 and 2, the rate equations in view of the Frumkin adsorption isotherm are given as

$$i_c = i_o(1-\theta_H)\exp(-a\alpha\eta)\exp(-\alpha f\theta_H) \tag{10}$$

$$i_r = Fk_2\theta_H^2\exp(2\ \alpha f\,\theta_H) \tag{11}$$

The generalized IPZ analysis contains two major relationships in addition to Equations 7 and 8 of the original IPZ analysis. These relationships are presented in Equations 12 and 13.

$$\ln\left(\frac{\sqrt{i_r}}{i_\infty}\right) = \ln\left(\sqrt{\frac{k_2}{F}} * \frac{1}{k''}\right) + \frac{\alpha f}{Fk}\,i_\infty \tag{12}$$

$$\frac{\sqrt{i_r}}{i_\infty}\,i_c\exp(a\alpha\eta) = \sqrt{\frac{k_2}{F}} * \frac{i_o'}{k} - \sqrt{\frac{k_2}{F}} * \frac{i_o'}{k} * \frac{i_\infty}{Fk} \tag{13}$$

Some progress toward the development of Equation 12 was made by Iyer, et. al. (1, 10). The rest of the development was accomplished during this past year on this project, and

yielded Equations 12 and 13. Plots of both $\ln(\frac{\sqrt{i_r}}{i_\infty})$ and $\frac{\sqrt{i_r}}{i_\infty}$ $i_c\exp(a\alpha\eta)$ vs. i_∞ should give straight lines according to Equations 12 and 13.

Results and Discussions

The effect of hydrogen sulfide in the charging solution on the relation between the measured steady state hydrogen permeation current density, i_∞, and the cathodic potential, E, on the input surface of the membrane in the charging compartment of the cell is presented in Figure 2. The figure shows that hydrogen sulfide strongly enhances hydrogen absorption into iron since the steady state hydrogen permeation current density increases by more than an order of magnitude with increasing H_2S concentration at the same cathodic potential. Figure 3 shows the effect of hydrogen sulfide concentrations in the charging solution on the relation between the rate of the hydrogen evolution reaction, i_c, on the input surface of the membrane and its potential, E. The figure reveals that hydrogen sulfide enhances the HER since the hydrogen overpotential is less (E is more positive) at the same value of the applied cathodic charging current.

Figure 4 shows the effect of hydrogen sulfide in the charging solution on the hydrogen concentration inside the membrane. This figure reveals that the hydrogen concentration inside the membrane increases as the hydrogen sulfide concentration increases in the charging solution.

Figure 5 shows the relation between the measured steady state hydrogen permeation current density, i_∞, and the square root of the recombination current density, $\sqrt{i_r}$, on the input side obtained at different hydrogen sulfide concentrations in the charging solution. This figure shows straight lines but only the line for the blank solution passes by the origin in accord with Equation 5. In the presence of hydrogen sulfide, the lines do not pass through the origin but rather have a finite intercept with the y-axis. This indicates that the original IPZ analysis can not be used to evaluate the data in the presence of hydrogen sulfide. Thus, it was clear that the IPZ analysis needed to be further developed in order to apply it to the iron/H_2S-acid system. As reported above, this model development was pursued in the past year and was successful.

Figure 6 shows the relation between $\ln(\frac{\sqrt{i_r}}{i_\infty})$ and the measured steady state hydrogen permeation current density, i_∞. The Figure shows straight lines in accord with Equation 12. Figure 7 shows linear relations between $\frac{\sqrt{i_r}}{i_\infty}$ $i_c \exp(a\alpha\eta)$ and the measured steady state hydrogen permeation current density, i_∞, in accord with Equation 13. This indicates that the newly developed generalized IPZ analysis can be used to analyze the data obtained with hydrogen sulfide present in the charging solution.

The slopes of the lines in Figure 7 were used along with the intercepts for the values of the kinetic-diffusion constant, k, according to Equation 13. The values of k at different hydrogen sulfide concentrations were used to estimate the hydrogen recombination rate constant, k_2, and the rate of change of the standard free energy of adsorption, f, from the intercepts and slopes of the lines in Figure 6 respectively, in accord with Equation 12. Values of k and k_2 were used to calculate the hydrogen exchange current density at different hydrogen sulfide concentrations, $i_o = \frac{i_o'}{(1-\theta_H^e)} = i_o'$ when $\theta_H^e << 1$, from the intercepts of Figure 7, in accord with Equation 13. The calculated values of the exchange current density were used to estimate the discharge rate constant, k_1, at different hydrogen sulfide concentration using the relation $i_o' = Fk_1C_{H^+}$ (7, 9).

Table 1 shows values for i_o, k_1, k_2, k and f at different hydrogen sulfide concentrations. These results show that hydrogen sulfide increases the proton discharge rate constant, k_1, and decreases the recombination rate constant of the HER, k_2. This could lead to an increase in the hydrogen surface coverage, θ_H. The values of k were used to estimate the hydrogen surface coverage, θ_H, using Equation 7 at different potentials and hydrogen sulfide concentrations. Figure 8 shows the relations between the hydrogen surface coverage, θ_H, and cathodic potential, E. It reveals that the hydrogen coverage increases with the increase in both hydrogen sulfide concentration and the potential in the cathodic direction.

Table 1 also shows that hydrogen sulfide affects also the rate of change of the standard free energy, f. The value of f increased from almost zero (0.20) in the absence

of hydrogen sulfide to nearly 9.0 in the presence of hydrogen sulfide. This indicates that the standard free energy of adsorption is coverage dependent, and that the Frumkin adsorption isotherm was correctly applied.

The increase in the hydrogen surface coverage, θ_H, and the rate of change of standard free energy of adsorption, f, dominate over the decrease in the hydrogen recombination rate constant of the HER, k_2, which leads to an increase in the hydrogen evolution reaction rate. However, the increase in the hydrogen absorption reaction rate is attributed to increases in the hydrogen surface coverage, θ_H, and the kinetic-diffusion constant, k.

Conclusions

The effect of hydrogen sulfide on the hydrogen absorption by iron was investigated using sodium sulfide as a source for the hydrogen sulfide during the experiments. Hydrogen sulfide enhanced both the HER and HAR on iron, in agreement with the findings of others. A generalized IPZ analysis was developed and then successfully used to analyze the hydrogen permeation data. This analysis shows that a presence of hydrogen sulfide in the electrolyte leads to the following effects:

a- An increase in the discharge rate constant of the HER, k_1, and hence in the exchange current density, i_o.

b- A decrease in the recombination rate constant of the HER, k_2.

c- An increase in the hydrogen surface coverage, θ_H.

d- An increase in the kinetic-diffusion constant of the HAR, k and

e- An increase in the rate of change of the standard free energy of adsorption, f.

Accordingly, the above data reveal that the increase in the hydrogen absorption rate in the presence of hydrogen sulfide is caused by an increase in the kinetic-diffusion constant, k and the hydrogen surface coverage, θ_H. The increase in θ_H is caused by an increase in the rate of the proton discharge step of the HER, k_1, and a decrease in the recombination rate constant of the HER, k_2. The enhancing effect of hydrogen sulfide on

the HER is due to the increases in k_1, θ_H, and the rate of change of the standard free energy of adsorption, f.

REFERENCES

1. R. N. Iyer, I. Takeuchi, M. Zamanzadeh, and H. W. Pickering, Corrosion, **46**, 460 (1990).

2. J. O'M. Bockris, J. McBreen, and L. Nanis, J. Electrochem. Soc., **112**, 1025 (1965).

3. T. R. Radhakrishnan and L. Shreir, Electrochim. Acta, **11**, 1007 (1966).

4. C. D. Kim and B. E. Wilde, J. Electrochem. Soc., **118**, 202 (1971).

5. M. A. Devanathan and Z. Stachurski, J. Electrochem. Soc., **111**, 619 (1964)

6. B. G. Ateya and H. E. Abd Elal, in Corrosion - Industrial Problems, Treatment and Control Techniques, V. Ashworth, Editor, p. 201, Conf. Proc., Kuwait Foundation for the Advancement of Science Proc. Series, Pergamon Press (1987).

7. R. Iyer, H. W. Pickering, and M. Zamanzadeh, J. Electrochem. Soc., **136**, 2463 (1989).

8. E. G. Dafft, K. Bohnenkamp and H. J. Engell, Corros. Sci., **19**, 591 (1979)

9. M. Ramasubramanian, B. N. Popov, and R. E. White, J. Electrochem. Soc, **145**, 1907 (1998).

10. R. N. Iyer and H. W. Pickering, "Mechanism and Kinetics of Electrochemical Hydrogen Entry and Degradation of Metallic Systems," Annual Review of Materials Science, Vol. 20, Annual Reviews, Inc., Palo Alto, Calif., (1990).

Table 1: Values of k, k_2, i_o, k_1, and f obtained on iron membrane at different hydrogen sulfide concentrations at pH 2.

H_2S Content	k mol $cm^{-2} s^{-1}$	k_2 mol $cm^{-2} s^{-1}$	i_o $\mu A\ cm^{-2}$	k_1 cm s^{-1}	f
Blank	7.02×10^{-11}	4.96×10^{-8}	0.421	4.36×10^{-7}	0.49
50 µM	6.61×10^{-10}	2.82×10^{-9}	2.78	2.89×10^{-6}	8.94
500 µM	9.62×10^{-10}	2.66×10^{-9}	9.22	9.56×10^{-6}	8.87
5 mM	1.43×10^{-9}	9.24×10^{-10}	26.1	2.70×10^{-5}	8.26

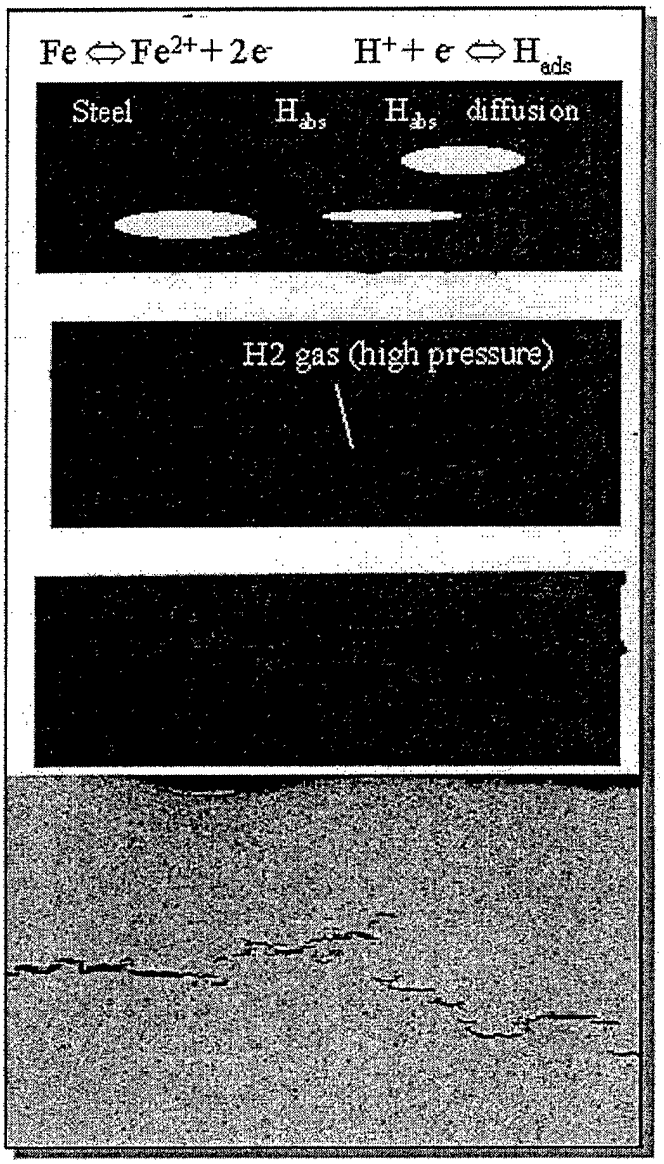

Fig. 1: Illustration of hydrogen builds up and crack propagation by HIC

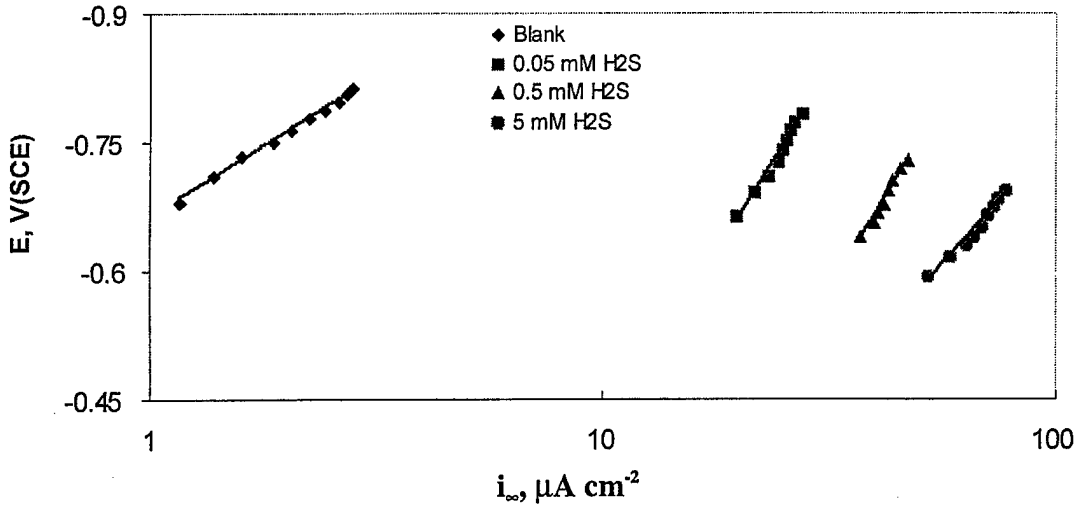

Fig. 2: The relation between the measured steady state hydrogen permeation current density, i_∞, and the electrode potential (E) obtained at different hydrogen sulfide concentrations at pH 2.

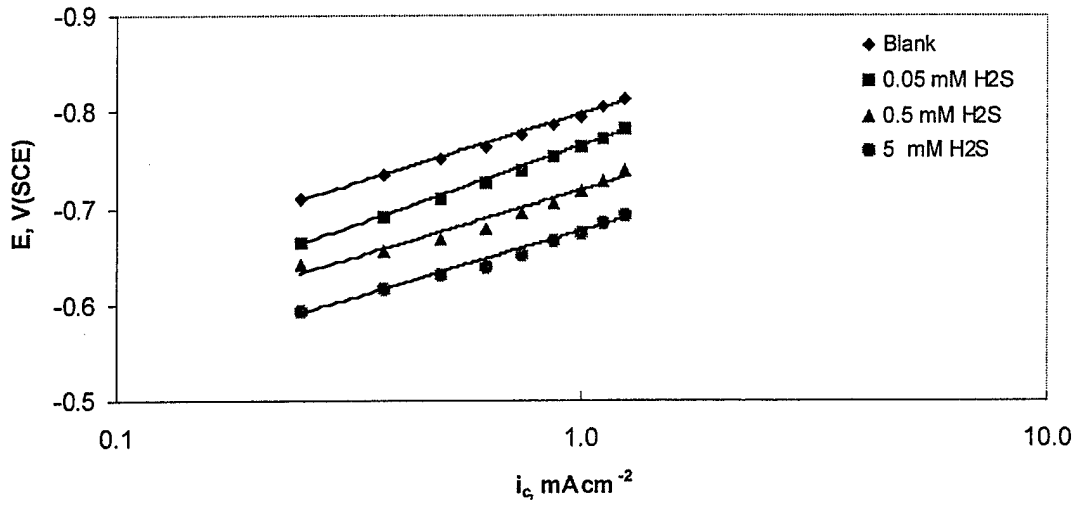

Fig. 3: The relation between the charging current density (i_c) and the electrode potential (E) obtained at different hydrogen sulfide ion concentrations at pH 2.

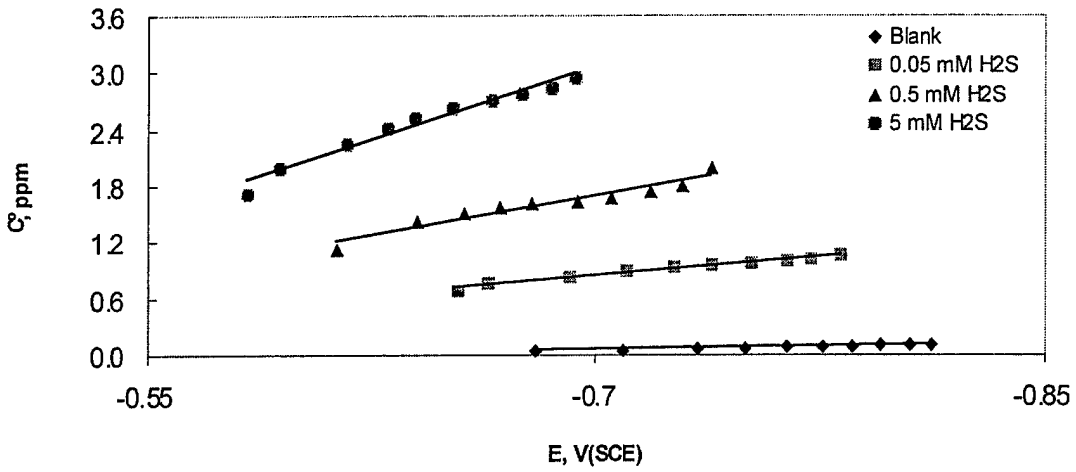

Fig. 4: The relation between the hydrogen concentration inside the membrane (C^o) and the electrode potential (E) obtained at different hydrogen sulfide ion concentrations at pH 2.

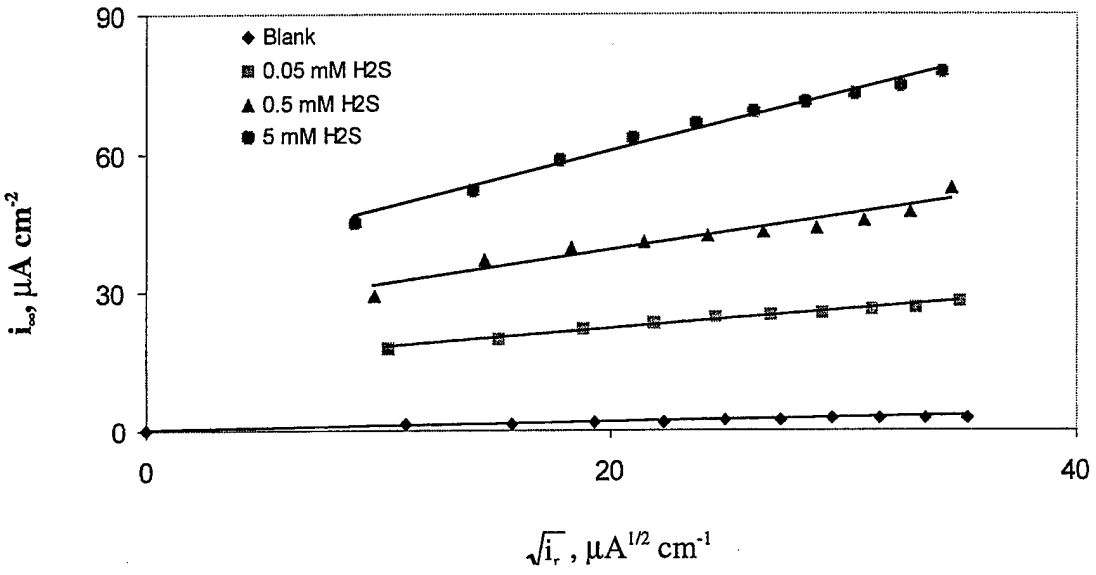

Fig. 5: The relation between the measured steady state hydrogen permeation current density, i_∞, and the square root of the hydrogen recombination current density, $\sqrt{i_r}$, obtained at different hydrogen sulfide concentrations at pH 2.

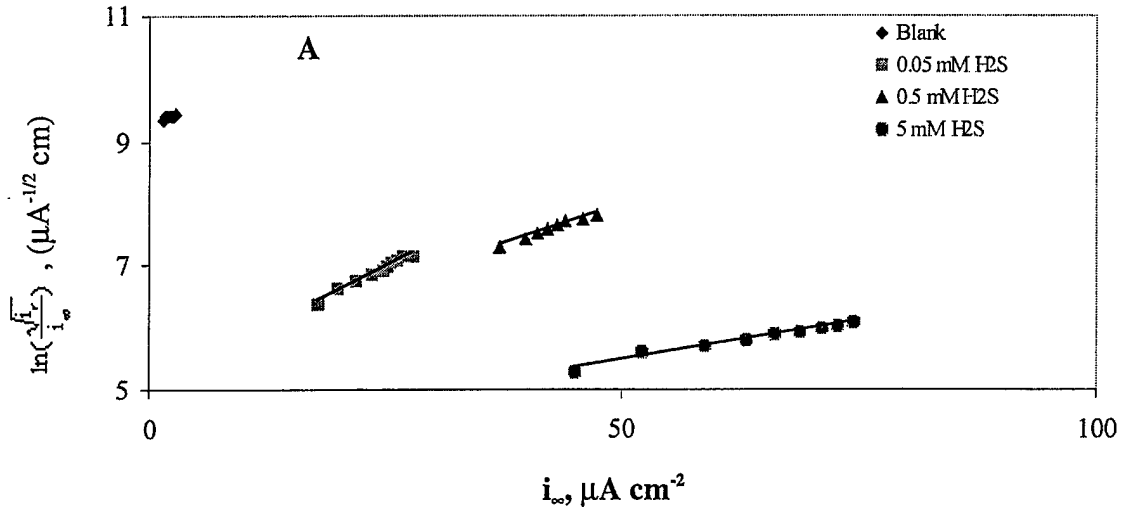

Fig. 6 The relation between $\ln(\frac{\sqrt{i_r}}{i_\infty})$ and the measured steady state hydrogen permeation current density, i_∞, obtained at different hydrogen sulfide concentrations at pH 2

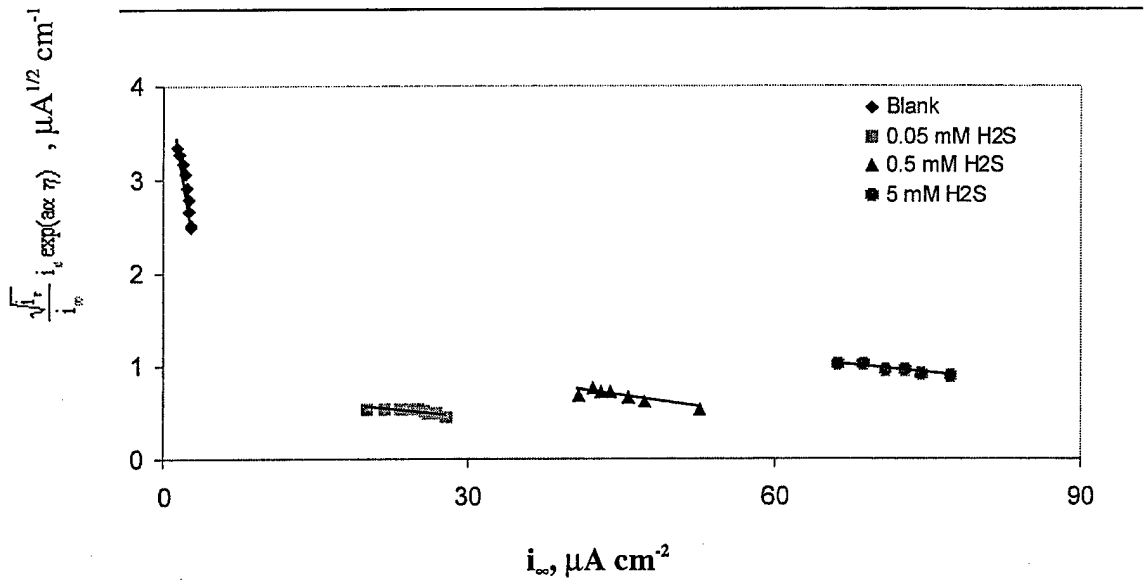

Fig. 7: The relation between $\frac{\sqrt{i_r}}{i_\infty} i_c \exp(a\alpha\eta)$ and the measured steady state hydrogen permeation current density, i_∞, obtained at different hydrogen sulfide concentrations at pH 2.

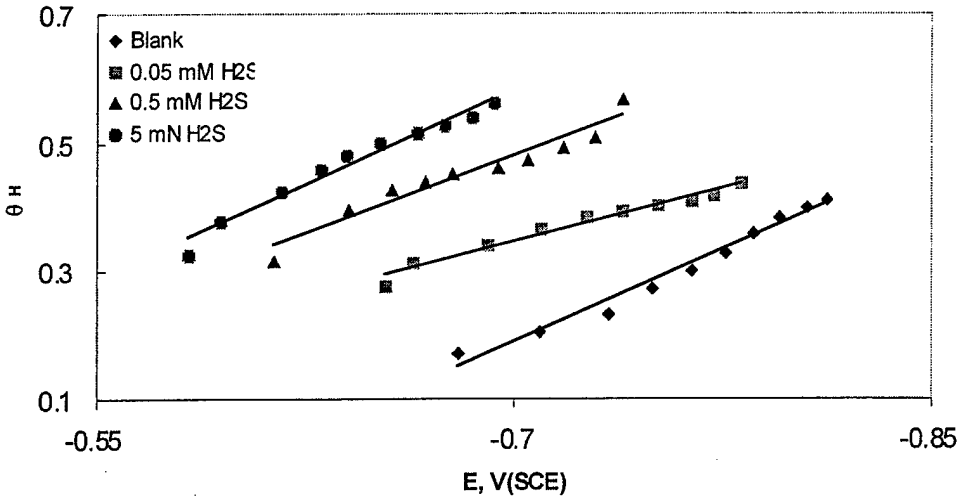

Fig. 8: The relations between the hydrogen surface coverage, θ_H, and electrode potential (E) obtained at different hydrogen sulfide concentrations at pH 2.

(3) Development and Testing of an Analytical Procedure for Quantitative Characterization of the HER from Polarization Data

The absorption of hydrogen into metals relies on the kinetics of the HER. Thus, a clear understanding of the HER would help in the understanding of the process of hydrogen absorption into metals. In this report we tried to understand the kinetics of the HER on metals from the fundamental point of view, i.e., by characterizing the reaction in terms of its hydrogen surface coverage and its kinetic rate constants. This involves the foundation of a new analysis that makes use of some of the pre-existing analyses in the literature to fully describe the HER. As will be shown later, this analysis, for the first time, uses the current-potential data to quantify the hydrogen evolution reaction on metals where the mechanism is Volmer-Tafel, using simple analytical equations.

Theoretical Background

Assume the HER proceeds by a Volmer discharge-Tafel recombination mechanism, i.e.,

$$H^+ + e^- + M \xrightarrow{k_1} M\text{-}H_{ads} \quad (1)$$

$$M\text{-}H_{ads} + M\text{-}H_{ads} \xrightarrow{k_2} 2M + H_2 \quad (2)$$

where $M\text{-}H_{ads}$ refers to an adsorbed hydrogen atom on the metal surface and k_1 and k_2 are the rate constants of the discharge and recombination steps of the HER, respectively. This adsorbed hydrogen is also involved in an absorption reaction, i.e.,

$$H_{ads} \leftrightarrows H_{abs} \quad (3)$$

where H_{abs} refers to the hydrogen absorbed within the lattice of the metal. A measure of a metal's tendency for absorbing hydrogen is its steady state rate of hydrogen permeation rate, i_∞. However, the i_∞ value could underestimate the absorption rate that occurs prior to steady state permeation, since the transient rate of hydrogen absorption can be much

higher than the steady state value, especially initially when there can exist a high density of unfilled traps for hydrogen in the metal, e.g., in the case of certain steels, or in the case of metals which exhibit high solubilities and/or diffusivities for hydrogen, e.g., palladium. Thus, if i_∞ data are used as a measure of hydrogen absorption, it is advisable that the following analysis be restricted in use to those metal/electrolyte systems for which i_∞ is orders of magnitude below i_c so that the absorption rate is insignificant at all times with respect to the rate of the HER.

At steady state the rate of generation of H_{ads} by reaction 1 (i_c) equals the sum of the rates of Reactions 2 (i_r) and 3 (i_∞), i.e.,

$$i_c = i_r + i_\infty \tag{4}$$

For some metals, such as the fcc metals copper and nickel, the permeabilities of hydrogen are typically very low in view of their low diffusivities for hydrogen in comparison to the rate of the HER, i.e., $i_c = i_r >> i_\infty$. This condition ($i_c \cong i_r$) could also hold for other metals like iron where the value of i_∞, though readily measurable, nevertheless is often some (2-3) orders of magnitude smaller than i_c. However, for iron in the presence of poisons such as hydrogen sulfide, the measured values of i_∞ are much higher and the assumption $i_c = i_r$ becomes less valid. Accordingly, if i_∞ is insignificant with respect to i_c, i_{abs} may also be insignificant with respect to i_c during measurement of the steady state polarization curve, in which case the analysis can yield the hydrogen surface coverage and the rate constants of the HER, as is shown below.

The rate of proton discharge (denoted i_c) in the Tafel region of the polarization curve is given by

$$i_c = Fk_1 C_{H^+} (1-\theta_H) \exp\left(-\frac{F}{RT}\alpha\eta\right) = i_o' (1-\theta_H) \exp\left(-\frac{F}{RT}\alpha\eta\right) \tag{5}$$

where $i_o' = Fk_1 C_{H+} = i_o/(1-\theta_H^e)$, i_o is the exchange current density of the HER at the limit of the equilibrium coverage, θ_H^e, C_{H^+} is the hydrogen ion concentration, α is the transfer

coefficient of the HER and η is the overpotential driving the HER. The rate of the recombination reaction, Eq. 2, is given by

$$i_r = Fk_2\theta^2_H \tag{6}$$

Rearranging Eq. 5 gives (20, 21):

$$i_c \exp(\frac{F}{RT}\alpha\eta) = i_o' (1-\theta_H) \tag{7}$$

The left hand side of Eq. 7 is called the charging function which combines the rate and driving force of the HER. Solving Eq. 6 for θ_H gives

$$\theta_H = \frac{\sqrt{i_r}}{\sqrt{Fk_2}} \tag{8a}$$

Inserting Eq. 4 with $i_\infty << i_c$, Eq. 8a becomes

$$\theta_H = \frac{\sqrt{i_c}}{\sqrt{Fk_2}} \tag{8b}$$

Combining Eqs. 5 and 8 yields:

$$i_c\exp(\frac{F}{RT}\alpha\eta) = i_o'(1-\frac{\sqrt{i_c}}{\sqrt{Fk_2}}) \tag{9}$$

Eq. 9 predicts a straight line relation between the charging function, $i_c\exp(\frac{F}{RT}\alpha\eta)$, and $\sqrt{i_c}$. From the slope $-\frac{i_o'}{\sqrt{Fk_2}}$ and the intercept (i_o') of this plot one obtains i_o' and k_2. From Eq. 5 at the limit of $\theta_H = \theta^e_H$ one has for $\theta^e_H = 0$,

$$i_o = Fk_1 C_{H^+}(1-\theta_H^e) = Fk_1 C_{H^+} \qquad (10)$$

While i_o can be inserted into Eq. 10 to calculate k_1, k_2 can be used to calculate the hydrogen surface coverage at different potentials, using Eq. 6, assuming $i_c = i_r$.

Experimental

Cathodic polarization experiments were carried out on copper samples of purity 99.5% and iron samples of purity 99.5% in 0.1N H_2SO_4+0.9N Na_2SO_4 (pH≈1.8), using an EG&G pontentiostat model 276. The samples were polished down to 0.5 μm alumina, rinsed with acetone and double distilled water. The test solutions were prepared from analytical grade chemicals and double distilled water. All solutions were pre-electrolyzed at 3mA for 2 hrs before measurements were taken. Before running the experiments the solutions were de-aerated using hydrogen to remove the dissolved oxygen from the solution. A conventional three electrode cell was used with saturated calomel as a reference electrode and two identical graphite rods as the counter electrodes.

Fig. 1 shows the Tafel plot obtained for hydrogen evolution on copper in 0.1N H_2SO_4 + 0.9N Na_2SO_4 at 25° C. The Tafel line has a slope of 121 mV (i.e., $\alpha \cong 0.5$) which is comparable to the values in the literature (22-25). Fig. 2 is a plot of the charging function, $i_c \exp(\frac{F}{RT}\alpha\eta)$, versus $\sqrt{i_c}$. It shows a satisfactory straight line with a negative slope and a positive intercept (see Eq. 9). Table 1 shows the values of the exchange current density, i_o, discharge rate constant, k_1, and the recombination rate constant, k_2, which were calculated using the slope and the intercept of the line in Fig. 2. The values are $i_o = 7.95 \times 10^{-8}$ A cm^{-2}, $k_1 = 4.96 \times 10^{-8}$ cm s^{-1} and $k_2 = 1.84 \times 10^{-7}$ mol cm^{-2} s^{-1}. The value of the recombination rate constant, k_2, was used to calculate the hydrogen surface coverage θ_H using Eq. 6. Fig. 3 shows the relation between θ_H and the electrode potential. This figure shows that the hydrogen surface coverage increases as the potential becomes less noble, i.e., as the overpotential for the HER increases. This trend is well documented in the literature (21, 26-34).

The present polarization analysis was also applied to the polarization curve of hydrogen evolution obtained on iron in deaerated 0.1N H_2SO_4 + 0.9N Na_2SO_4. Fig. 4 shows the relation between the charging function and the square root of the cathodic charging current obtained on iron. The charging function was calculated using a value of $\alpha = 0.5$ as measured in this work. This figure shows a straight line relation with a negative slope in accord with Eq. 9. A comparison is made in Table 1 between the values of the exchange current density and the rate constants obtained from this analysis and those obtained for this same system from steady state hydrogen permeation data using the Iyer-Pickering-Zamanzdeh (IPZ) analysis (35). The table shows that the present polarization analysis gives the same order-of-magnitude values as the IPZ analysis gives. The values of the hydrogen surface coverage estimated from the IPZ analysis were also compared with those obtained using the present analysis, see Fig. 5. This figure shows a good agreement in particular at the less noble potentials. At the more noble potentials, e.g., -0.63 V (35), the value of θ_H calculated in this work is approximately 15% lower than that obtained from the IPZ analysis.

The results presented herein show how the polarization data can be analyzed for the kinetic parameters (rate constants) and the hydrogen surface coverage of the HER on metals, where the hydrogen absorption rate is negligible with respect to the cathodic hydrogen evolution current density, i_c, such as in the case of copper and other metals that have low (insignificant) hydrogen absorption rates. Analysis of the results on copper gives a value for the exchange current density of the HER which is similar to those reported in the literature (22, 36, 37). It was shown that the hydrogen surface coverage changes with the potential in a trend that is well documented in the literature. The present polarization analysis of the data on iron gives values of the exchange current density, rate constants and values for the hydrogen surface coverage which are comparable to those obtained by the IPZ analysis.

This polarization analysis is clearly less applicable in cases where i_∞ is significant with respect to i_c, e.g., in the case of Pd which has a very high permeability for hydrogen, and iron in poisoned solutions where the presence of the poison significantly increases the rate of hydrogen absorption. It involves a limiting case of the IPZ analysis (20,21), where i_∞ is very small compared to i_c. A comparison between the results obtained on iron

using the IPZ and the present polarization analyses shows that both analysis procedures give the same order of magnitude values of the kinetic parameters (exchange current density and rate constants) and the hydrogen surface coverage. Being less than the complete IPZ analysis, the present polarization analysis can not predict the rate constants of the hydrogen absorption and desorption reactions.

References

1- J. O'M. Bockris, Chem. Rev., **43**, 525 (1948).

2- T. N. Veziroglu, H. J. Plass, and F. Barbir in Electrochemistry in Transition, O. J. Murphy, S. Srinivasan, and B. E. Conway, Editors, p. 325, Plenum Press, New York (1992).

3- B. G. Pound in Modern Aspects of Electrochemistry J. O'M. Bockris, B. E. Conway, and R. E. White, Editors, Vol. 25, p. 63 (1993).

4- G. Jerkiewicz, Progress in Surf. Sci., **57**, 137 (1998).

5- A. Lasia, Polish. J. Chem., **69**, 639 (1995).

6- J. O'M. Bockris, Inter. J. Hydr. Energ., **24**, 1 (1999).

7- K. J. Vetter, Electrochemical Kinetics, p. 525-535, Academic Press, New York (1967).

8- B. K. Subramanyan in Comprehensive Treatise of Electrochemistry, J. O'M. Bockris, B. E. Conway, E. Yeager, and R. E. White, Editors, Vol. 4, p. 411, Plenum Press, New York (1981).

9- S. Trasati in Advances in Electrochemical Science and Engineering, H. Gerischer and C. W. Tobias, Editors, Vol. 2, p.1, VCH, New York (1992).

10- R. L. Augustine in Catalytic Hydrogenation, p. 26, Marcel Decker, Inc., New York (1985).

11- Electrocatalysis, J. Lipkowski and P. N. Ross, Editors, Wiley-VCH, New York (1998).

12- C. A. McAuliffe, Hydrogen and Energy, Gulf Pub., Houston (1980).

13- D. Talbot and J. Talbot in Corrosion Science and Technology, CRC Press, Houston (1998).

14- T. Mizuno and M. Enyo in Modern Aspects of Electrochemistry, R. E. White, B. E. Conway, and J. O'.M. Bockris, Editors, Vol. 30, p. 451, Plenum Press, New York (1996).

15- M. A. Fullenweider in Hydrogen Entry and Action in Metals, Pergamon Press, New York (1983).

16- G. B. Nielsen, J. E. T. Andersen, and J. C. Reeve in Modern Aspects of Electrochemistry, R. E. White, B. E. Conway, and J. O'.M. Bockris, Editors, V. 31, p. 251, Plenum Press, New York (1997).

17- J. W. Dini in Electrodeposition, The Materials Science of Coatings and Substrates, Noyes Publications, NJ (1993).

18- H. Flitt and J. O'M. Bockris, Int. J. Hydr. Energ. **7**, 51 (1982).

19- J. O'M. Bockris, J. L. Carbajal, B. R. Scharifker, and K. Chandrasekaran, J. Electrochem. Soc., **134**, 1957 (1987).

20- R. N. Iyer, H. W. Pickering, and M. Zamanzadeh, J. Electrochem. Soc., **136**, 2463 (1989).

21- R. N. Iyer and H. W. Pickering, Annu. Rev. Mater. Sci., **20**, 299 (1990).

22- N. Pentland, J. O'M. Bockris, and E. Sheldon, J. Electrochem. Soc., **104**, 182 (1957).

23- J. O'M. Bockris and N. Pentland, Trans. Farad. Soc., **48**, 833 (1952).

24- S. Y. Lanina and Z. A. Iofa, Sov. Electrochem., **5**, 327 (1969).

25- D. Altura and K. Nobe, Corrosion, **28**, 345 (1972).

26- M. A. Devanathan, J. O'M. Bockris, and W. Mehl, J. Electroanal. Chem., **1**, 143 (1959).

27- C. D. Kim and B. E. Wilde, J. Electrochem. Soc., **118**, 202 (1971).

28- R. N. Iyer, I. Takauchi, M. Zamanzadeh, and H. W. Pickering, Corrosion, **46**, 360 (1990).

29- J. L. Carbajal and R. E. White, in Electrochemistry in Transition, O. J. Murphy, S. Srinivasan, and B. E. Conway, Editors, p. 339, Plenum Press, New York (1992).

30- D. H. Coleman, G. Zheng, B. N. Popov, and R. E. White, J. Electrochem. Soc., **143**, 1871 (1995).

31- B. E. Conway, J. H. Barber, L. Gao, and S. Y. Qian, J. Alloys and Compounds, **253**, 475 (1997).

32- H. A. Durtee, D. M. See, B. N. Popov, and R. E. White, J. Electrochem. Soc., **144**, 2313 (1997).

33- S. Y. Qian, B. E. Conway, and G. Jerkiewicz, J. Chem. Soc., Faraday Trans., **94**, 2945 (1998).

34- M. Ramasubramanian, B. N. Popov, and R. E. White, J. Electrochem. Soc., **145**, 1907 (1998).

35- M. H. Abd Elhamid, B. G. Ateya, and H. W. Pickering, Electrochem. Soc., **147**, 2258 (1999).

36- A. J. Appleby in Encyclopedia of Electrochemistry of the Elements, A. J. Bard, Editor, Vol. 4, p. 383, Marcel Decker, New York (1975).

37- A. T. Kuhn and C. J. Mortimer, J. Electroanal. Chem., **34**, 1 (1972).

List of Symbols

C_{H+} hydrogen ion concentration, mol cm^{-3}

F Faraday's constant, coul mol^{-1}

i_o' $=Fk_1C_{H+}=\frac{i_o}{(1-\theta_H^e)}$, A cm^{-2}

i_o exchange current density, A cm^{-2}

i_r steady state recombination current density, A cm^{-2}

i_p steady state hydrogen permeation current density, A cm^{-2}

k_1 discharge rate constant, mol s^{-1}

k_2 recombination rate constant, mol cm^{-2} s^{-1}

R general gas constant, 8.314 J mol^{-1} K^{-1}

T absolute temperature,K

Greek symbols

α transfer coefficient, dimensionless

η cathodic overvoltage, V

θ_H^e hydrogen surface coverage at equilibrium, dimensionless

θ_H hydrogen surface coverage, dimensionless

Table 1: Comparison of the exchange current density, discharge and recombination rate constants and the transfer coefficient for iron in 0.1N H_2SO_4 + 0.9N Na_2SO_4 obtained from the IPZ analysis (35,36) and the present polarization analysis. The same quantities were also obtained for copper using the polarization analysis.

Analysis	i_o, A cm^{-2}		k_2, mol cm^{-2} s^{-1}		k_1, cm s^{-1}		_	
	Fe	Cu	Fe	Cu	Fe	Cu	Fe	Cu
IPZ	2×10^{-6}	-	2.6×10^{-8}	-	1.3×10^{-6}	-	0.5	-
Present study	2×10^{-6}	8.0×10^{-8}	3.0×10^{-8}	1.8×10^{-7}	1.3×10^{-6}	5.0×10^{-8}	0.5	0.5

Figures Captions

Fig. 1 The relation between the cathodic current and the electrode potential obtained on copper in 0.1N H_2SO_4 + 0.9N Na_2SO_4.

Fig. 2 The relation between the charging function and the square root of the cathodic current obtained on copper in 0.1N H_2SO_4 + 0.9N Na_2SO_4.

Fig. 3 The relation between the hydrogen surface coverage and the electrode potential obtained on copper in 0.1N H_2SO_4 + 0.9N Na_2SO_4.

Fig. 4 The relation between the charging function and the square root of the cathodic current obtained on iron in 0.1N H_2SO_4 + 0.9N Na_2SO_4.

Fig. 5 The relation between the hydrogen surface coverage and the electrode potential obtained on iron in 0.1N H_2SO_4 + 0.9N Na_2SO_4 using the IPZ analysis and the present polarization analysis.

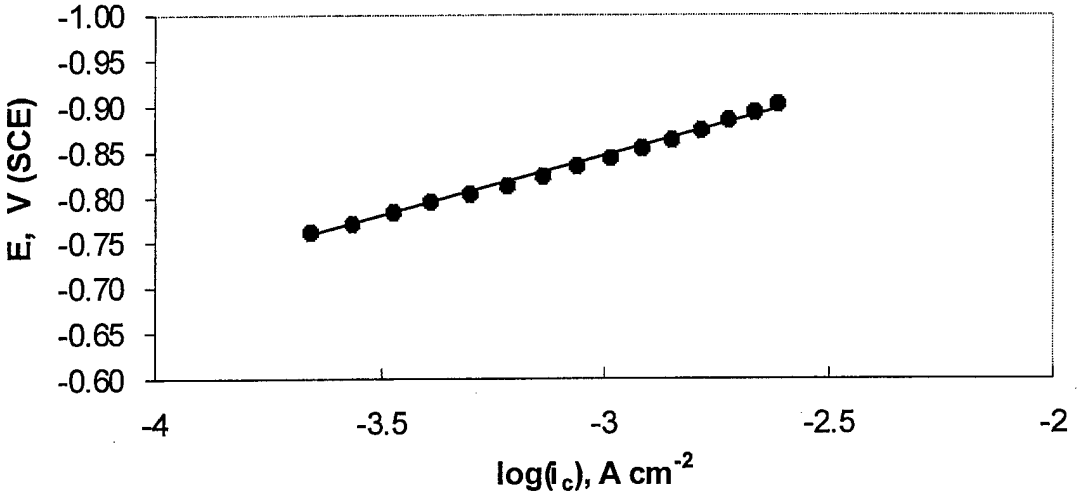

Fig. 1: The relation between the cathodic current and the electrode potential obtained on copper in 0.1N H_2SO_4 + 0.9N Na_2SO_4.

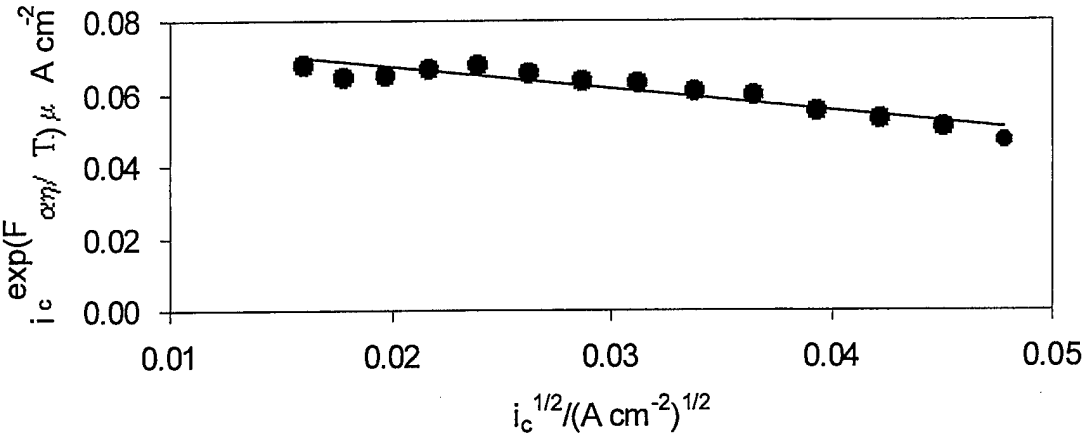

Fig. 2: The relation between the charging function and the square root of the cathodic current obtained on copper in 0.1N H_2SO_4 + 0.9N Na_2SO_4.

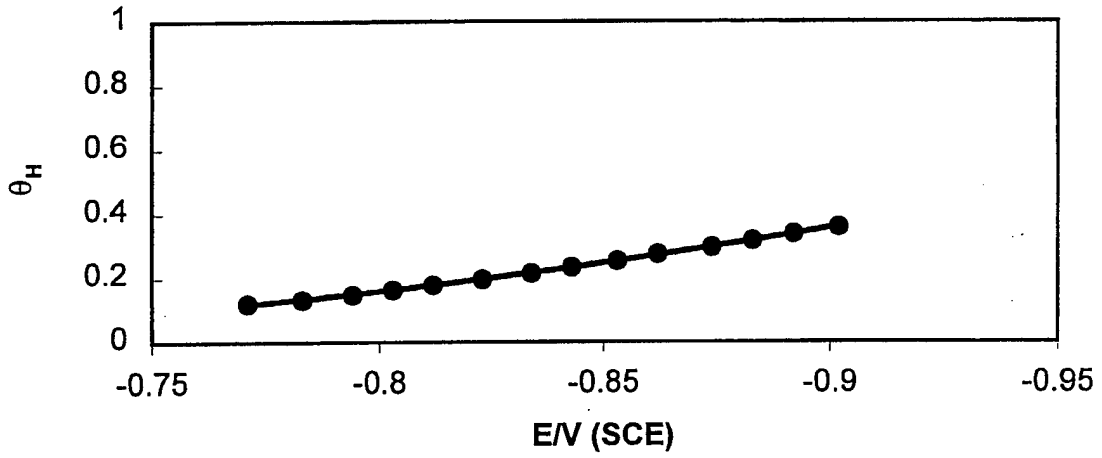

Fig. 3: The relation between the hydrogen surface coverage and the electrode potential obtained on copper in 0.1N H_2SO_4 + 0.9N Na_2SO_4.

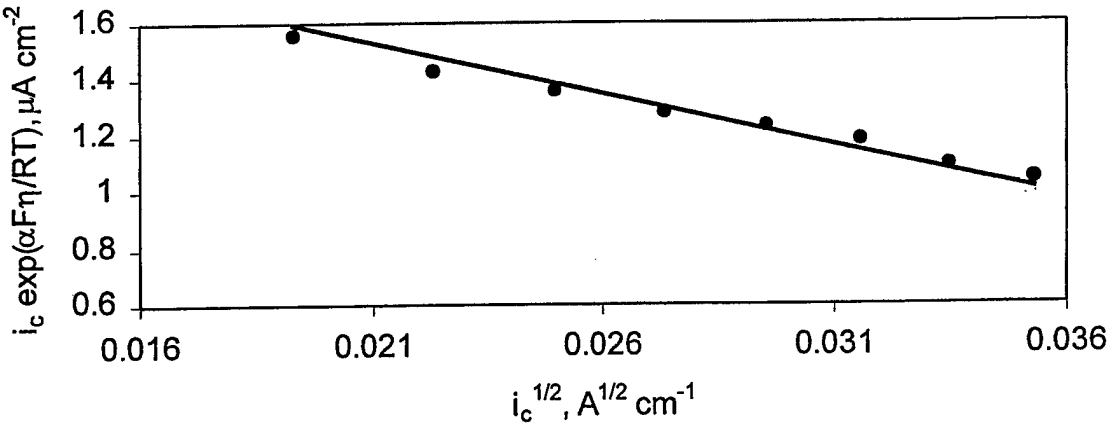

Fig. 4: The relation between the charging function and the square root of the cathodic current obtained on iron in 0.1N H_2SO_4 + 0.9N Na_2SO_4.

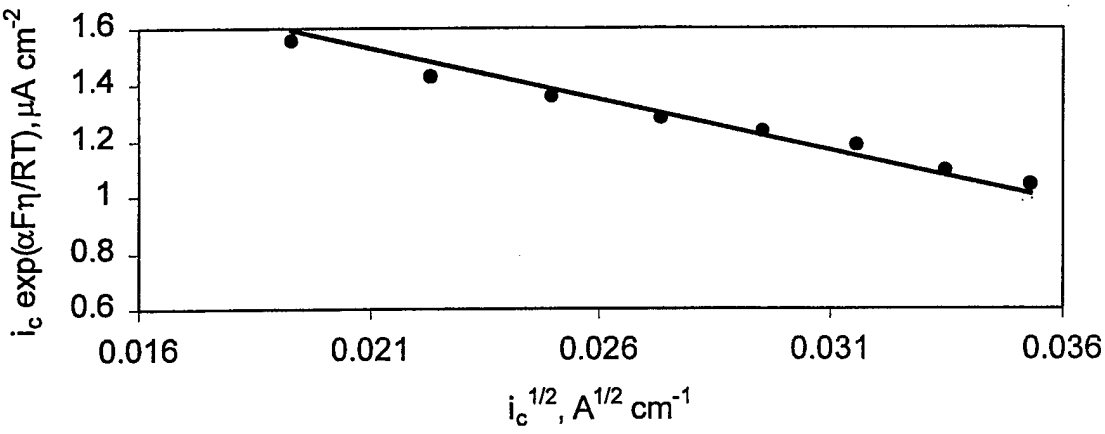

Fig. 4: The relation between the charging function and the square root of the cathodic current obtained on iron in 0.1N H_2SO_4 + 0.9N Na_2SO_4.

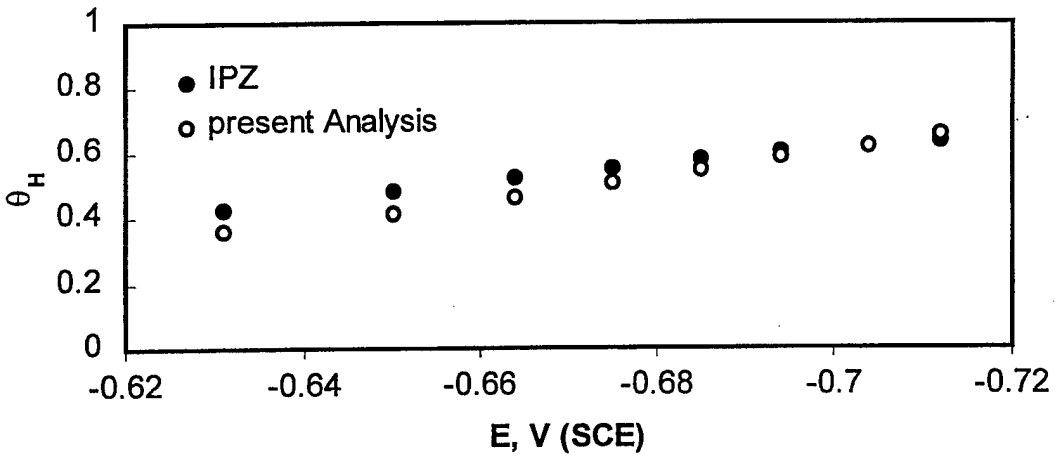

Fig. 5: The relation between the hydrogen surface coverage and the electrode potential obtained on iron in 0.1N H_2SO_4 + 0.9N Na_2SO_4 using the IPZ analysis and the present polarization analysis.

Reports Distribution

Addresses	Number of Copies
Office of Naval Research Program Officer A. John Sedriks ONR 332 Ballston Centre Tower One 800 North Quincy Street Arlington, VA 22217-5660	3
Administrative Grants Office OFFICE OF NAVAL RESEARCH REGIONAL OFFICE CHICAGO 536 S. Clark Street, Room 208 Chicago, IL 60605-1588	1
Director, Naval Research Laboratory ATTN: Code 2627 4555 Overlook Drive Washington, DC 20375-5326	1
Defense Technical Information Center 8725 John J. Kingman Road STE 0944 Ft. Belvoir, VA 22060-6218	2